



Synthesis, characterization and photocatalytic activity of CaZrO_3 - SiO_2 nanocomposite for the decolorization of indigo carmine dye

Neda Kermani^a, Seyed Saeed Mirzaee^b, Mohammad Ebrahim Olya^c,
Sayed Mohammad Javad Mirzaei^{d,*}

^aChemistry Department, Islamic Azad University Tehran North Branch, Tehran, Iran, email: Kermani_neda@yahoo.com (N. Kermani)

^bDepartment of Ceramic, Materials and Energy Research Centre, Karaj, Iran, email: s_mirzaee81@yahoo.com (S.S. Mirzaee)

^cDepartment of environmental research, Institute for colour science & technology, Tehran, Iran, email: me.olya@gmail.com (M.E. Olya)

^dDepartment of Water Engineering, Faculty of Agriculture and Animal Sciences, University of Torbat-e Jam, Torbat-e Jam, Iran, Tel. 989155016090, email: javadm_61@yahoo.com (S.M.J. Mirzaei)

Received 8 October 2017; Accepted 6 August 2018

ABSTRACT

The photocatalytic decolorization of indigo carmine (acid blue 74) in an oxidation process was studied using a silica- calcium zirconate (CZS) powder as a semiconductor photocatalyst in a batch reactor equipped with a 15W low-pressure mercury lamp. The effects of various influential parameters including initial dye concentration, photocatalyst dose, pH, temperature and stirring rate on the dye decolorization were also optimized. The optimum value of initial dye concentration, photocatalyst concentration and stirring rate were 5 ppm, 0.04 g/L, and 600 rpm, respectively. Furthermore, the maximum decolorization was observed at the pH of 3. X-ray diffraction (XRD) and infrared spectra (FT-IR) techniques were used to confirm the formation of photocatalyst. The particle size and specific surface area of photocatalyst were determined by scanning electron microscopy (SEM) and Brunauer-Emmett-Teller (BET) theory. UV-Vis spectroscopy was employed to evaluate the dye degradation and LC-MS technique was used to evaluate the formation of the intermediate compounds. The results indicate that silica-calcium zirconate nanocomposite is suitable for the degradation of organic pollutants from wastewater.

Keywords: Photocatalysis; Decolorization; Acid Blue 74; Calcium zirconate; Textile industry wastewater

1. Introduction

Throughout history, fabrics have been dyed with extracts from plants and animals. However, dying industry began to change with the discovery of synthetic dyes. These dyes were easy to apply, had lower costs, and offered an extensive range of colors. Too many dyes (which are resistant to chemicals and light) are used in textile industry [1,2], food technology [3,4], hair colors [5], leather tanning [6,7], plastic [8] and paper production [9,10]. These compounds show significant structural diversity.

Synthetic dyes can be classified based on their particular chromophoric group. Indigoid, azo, anthraquinone, triphenylmethyl, sulfur, and phthalocyanine are the most commonly used dyes in the industry. More than half (up to 70%) of the synthesized dyes belongs to the azo(-N=N-) group. The major drawback to these chemicals is their toxic, non-biodegradable properties [11]. Thus, they cause severe pollution problems by releasing carcinogenic compounds into the environment, and affect the aquatic cycle balance and ecosystem [12].

Indigo carmine is a cationic dye which is extensively used in cosmetics, drugs and the food industry. In spite of the several advantages of this compound such as helping to

*Corresponding author.

target biopsies [13] and in the diagnosis of Barrett's esophagus [14], the results showed that it can be harmful to human health. Therefore, the elimination of indigo carmine from effluents is necessary. For instance, it was observed that indigo carmine causes strong clastogenic activity on bone marrow chromosomes of mice [15].

To avoid the accumulation of synthetic dyes in the wastewater, a variety of conventional methods such as flocculation, ultra-filtration, coagulation, sedimentation, and ozonation has been employed to remove the dye effluent [16–19]. However, these methods exhibit high operational costs. Advanced oxidation technology (AOT) can be a promising method due to its non-selectivity hydroxyl radical (OH^\bullet) formed. Therefore, it can be used to oxidize a wide range of pollutants into non-toxic compounds [20–22]. This process is used to degrade contaminants using light and semiconductor in an economical and environmentally friendly manner [23]. The most popular semiconductor materials used in the photocatalytic process are TiO_2 and ZnO [24,25]. At the present, many researches have been conducted to find new high-performance materials.

In the current study, silica-calcium zirconate nanocomposite (CZS) was synthesized and photocatalytic decolorization of indigo carmine (Acid Blue 74) was studied in a batch photo-reactor. Moreover, the most effective parameters such as photocatalyst concentration, pH, temperature, stirring rate and initial dye concentration at different irradiation times was investigated and finally the kinetic and the energy consumption of the process was evaluated.

2. Materials and methods

2.1. Reagents

The following reagents were used without further purification: Indigo carmine (Saujanya) (Table 1), stearic acid (Merck), calcium acetate (Merck), zirconium butoxide (Sigma Aldrich), and silicon dioxide (Razi Advanced Materials).

2.2. Equipment

The absorbance and change of dye concentration was determined using a UV-Vis spectrometer (Perkin Lambda

25) at the wavelength of 610 nm, which is the maximum wavelength of indigo carmine. The calibration curve was prepared from dye solutions with different concentrations ($R^2 = 0.999$). During UV irradiation, sample solutions (5 mL) were taken from the photo reactor every 15 min until clear solution obtained. Then the samples were centrifuged at 12000 rpm for 10 min and separated the CZS catalyst. HPLC separation was performed using an Agilent 6410 system equipped with a diode array detector (D.A.D). For the identification of photocatalytic reaction intermediates a C18 column (250×4.6 mm, 5 μm) was used. The mobile phase was consisted of 10:90 (v/v) methanol: water. The injection volume used was 20 μL and flow rate was 0.6 mL/min. The wavelength monitored by D.A.D. analyzer was 254 nm.

3. The experiment

3.1. Photocatalyst preparation

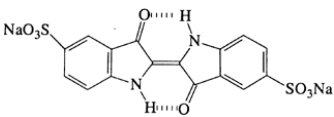
Silica-calcium zirconate was used in this research as a photocatalyst. This chemical compound was synthesized via sol-gel method. As was described in our previous work [26], zirconium butoxide and calcium acetate with the molar ratio of 1:1 were first dissolved in stearic acid. Then 80% wt. silica was added to the prepared calcium zirconate sol. Gelation process took place at a while. After dried at 80°C for 5 h in an oven, it was calcined at 900°C for 4 h and the silica-calcium zirconate nanocomposite was successfully synthesized.

3.2. Photocatalyst characterization

3.2.1. X-ray diffraction (XRD)

The preparation of silica-calcium zirconate nanocomposite was evaluated by XRD analysis. The X-ray diffraction study was carried out in the using Philips D500 diffractometer with $\text{Cu K}\alpha$ radiation operating at 30 mA and 40 kV at a scanning range of 10–80° with a scan rate of 4.8°/min. XRD pattern is presented in Fig. 1. The pattern was identified using expert PANalytical high score software. Silica (JCPDS card No. 01-085-0457) and calcium zirconate (JCPDS card

Table 1
Structure and characteristics of indigo carmine

Name	Indigo carmine
Formula	$\text{C}_{16}\text{H}_8\text{N}_2\text{Na}_2\text{O}_8\text{S}_2$
Molecular structure	
Structure type	Acidic
λ_{max} (nm)	610
Molecular weight ($\text{g}\cdot\text{mol}^{-1}$)	466.36
pKa	12.2

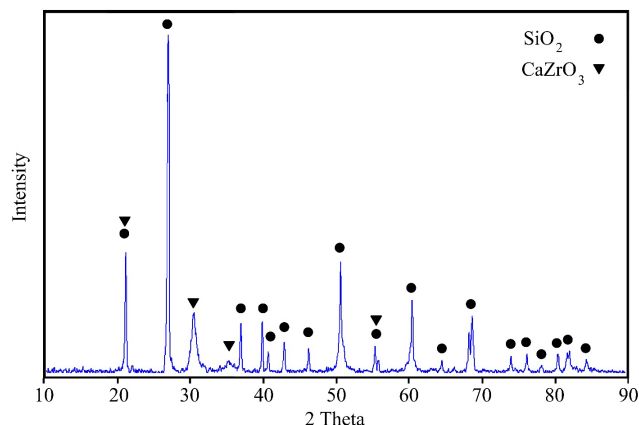


Fig. 1. XRD pattern of silica-calcium zirconate nanocomposite (CZS).

No. 01-076-2401) phases were detected, indicating nanocomposite formation.

3.2.2. Scanning electron microscopy (SEM)

The morphology of synthesized aerogel was examined by Philips XL30 field emission electron microscope. The SEM image of silica- calcium zirconate nanocomposite is illustrated in Fig. 2. It can be estimated that the average particle size is less than 100 nm, which is in accordance with the particle size distribution analysis (mean particle size = 75 nm). The observation confirmed discrete particles with acceptable spherical morphologies.

3.2.3. FTIR spectroscopy

Fourier transform infrared spectra (FTIR) was employed to study the chemical bond formation using Bruker-Vector 22 in the range 400–4000 cm^{-1} with resolution of 4 cm^{-1} . Fig. 3 represents FT-IR spectra of silica- calcium zirconate nanocomposite. In this spectrum, all the peaks are char-

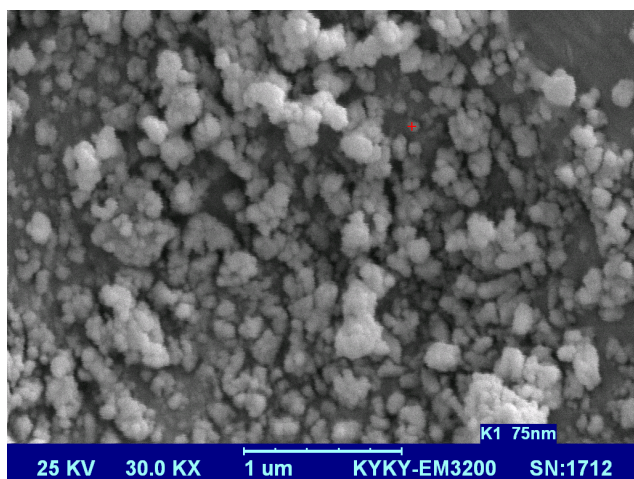


Fig. 2. Scanning electron microscopy of silica- calcium zirconate nanocomposite (CZS).

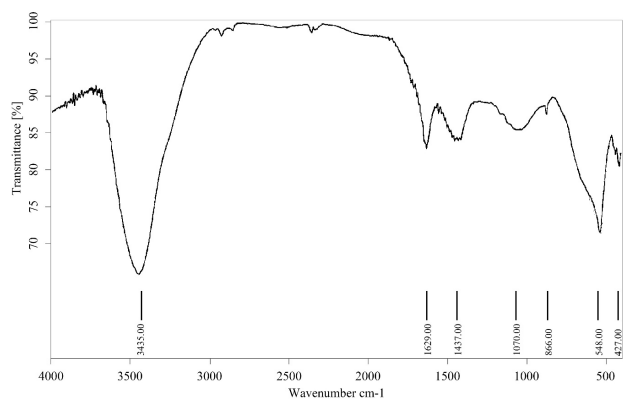


Fig. 3. FT-IR spectra of silica- calcium zirconate nanocomposite (CZS).

acteristics of the CaZrO_3 except the peaks at 1070 cm^{-1} and 3435 cm^{-1} which is due to the presence of silica matrix and adsorbed moisture. On the other hand, this figure reveals that there are no remaining organic compounds [27,28].

3.2.4. Band gap determination

The band gap (eV) is related to the electric conductivity and hence the energy gap (E_g) which is an important characteristic of the semiconductors. In fact, the band gap shows the difference in energy between the top of the valence band filled with electrons and the bottom of the conduction band, which has no electrons. This means that metals generally have no band gap and semiconductors have an intermediate band gap between the metals and isolators, which have a wide band gap. In this study, band gap energy was calculated according to the following equation [29]:

$$\alpha h\nu = C_1 (h\nu - E_g)^{1/2} \quad (1)$$

where α is the linear absorption coefficient of the substance, $h\nu$ is the photon energy, and C_1 is the proportionality constant. It can be seen from Tauc plot (Fig. 4) that at high values of $(\alpha h\nu)^2$ the plot follows a linear pattern, however, as $h\nu$ reaches lower values, the graph tends to deviate from its linear form.

In order to calculate the direct band gap, linear part of the graph was extrapolated on $h\nu$ axis, at $(\alpha h\nu)^2 = 0$. Direct band gap value for silica- calcium zirconate photocatalyst turned out to be 3.3 eV according to the above plot.

3.2.5. Textural analysis

The nitrogen adsorption/desorption was performed on Belsorp mini-II and the surface area of aerogel was calculated using Brunauer-Emmett-Teller (BET) method and pore size distribution and total pore volume was determined by the BJH model. The physical properties on the specific surface area, total pore volume and average pore diameter measured from the composite were 3.43 m^2/g , 0.005 cm^3/g and 6.83 nm respectively.

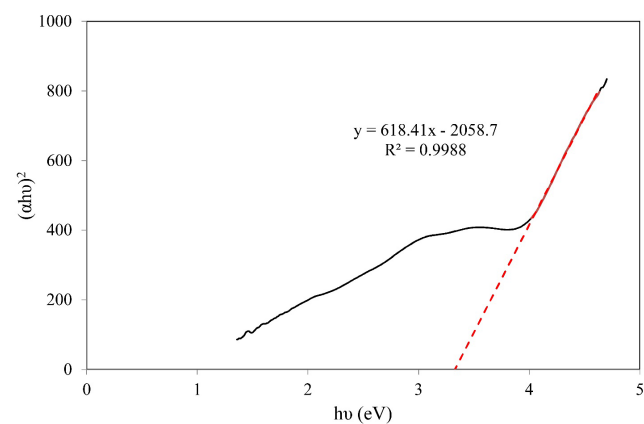


Fig. 4. Tauc plot for evaluation of direct band gap of silica- calcium zirconate nanocomposite (CZS).

3.3. Decolorization of dye

Photochemical decolorization of the synthetic dye solution was performed using silica calcium zirconate nanocomposite. At first, the solution was prepared by dissolving the required amount of dye in distilled water. Photocatalyst powder was then introduced into the dye solution. The aqueous mixture was magnetically stirred to keep the solution homogeneous and was subjected to photocatalytic decolorization. For this process, 2 L of prepared suspension was poured into a glass reactor equipped with UV lamp (15W), which was switched on at the beginning of the process. The schematic diagram of the experimental apparatus is shown in Fig. 5. Ultimately, residual acid Blue 74 concentration in aqueous solution was measured at the wavelength of 610 nm. The decolorization efficiency (%) was determined by Eq. (2), where C_0 (mg/L), and C (mg/L) are the concentration of dye before and after photocatalysis, respectively.

$$\% \text{ efficiency} = \frac{C_0 - C}{C_0} \times 100 \quad (2)$$

In this process, the effect of main operating variables such as initial dye concentration, photocatalyst dose, pH, temperature and stirring rate on the removal of indigo carmine were investigated. The initial conditions of the experiment were as follows: photocatalyst concentration of 0.04 g/L, pH of 7, temperature of 27°C, stirring rate of 600 rpm, dye concentration of 5 ppm and irradiation time of 60 min. To determine the effect of silica- calcium zirconate amount on the dye elimination, various concentrations of photocatalyst were used (0.01, 0.02, 0.03, 0.04, 0.05, and 0.06 g/L). The effect of indigo carmine concentration on the removal efficiency was also studied by applying different quantities of dye (5, 10, 20, and 30 ppm). The role of pH on the decolorization process was determined at diversity of values (3, 5, 7, and 9), which the pH adjustment was carried out using 0.2 M NaOH and HCl solutions. The effect of stirring rate was also evaluated at three rates of 200, 400, and 600 rpm. The effect of temperature was measured at 27, and 32°C. Each experiment was repeated twice and the average

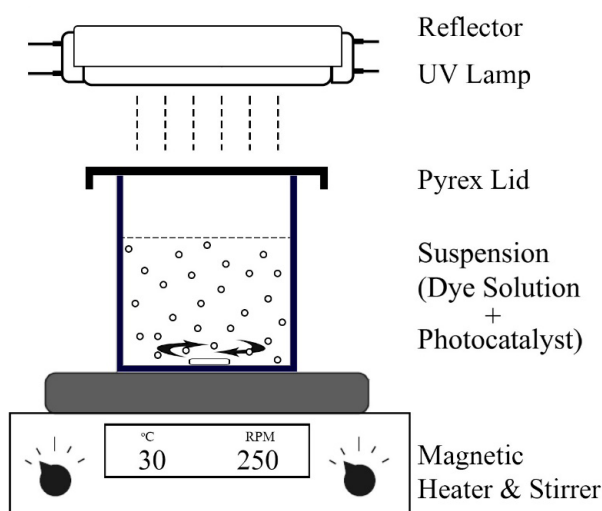


Fig. 5. Schematic diagram of photoreactor.

results were reported. If there were out of range results, a confirmation test was performed.

4. Results and discussion

4.1. Effect of photocatalyst concentration

The effect of photocatalyst concentration on decolorization of dye was studied in a 0.5 ppm acid blue 74 solution at pH of 3. The rate of stirring and temperature of the experiment were kept at 300 rpm and 27°C, respectively. Fig. 6 shows that the decolorization of synthetic dye increases with higher amounts of nanocomposite. The maximum amount of dye removal was observed at catalyst concentration of 0.04 g/L. This can be explained by the fact that with the increase of photocatalyst amount, the active surface area increases as well. Therefore, more active sites will be available on photocatalyst surface, which in turn increases the number of OH^\bullet and $\text{O}_2^{\bullet-}$ radicals. Also, higher amount of photocatalyst leads to an increase in turbidity of suspension, which results in decrease of UV light penetration and thus decrease in the photoactivated volume of suspension [30].

4.2. Effect of pH

Fig. 7 shows the decolorization of dye with increasing pH under different irradiation times. It can be seen that in all irradiation times, the decolorization decreases as the pH increases. The maximum decolorization was observed in acidic medium. The surface of photocatalyst becomes positively charged in acidic condition, resulting in adsorption of anionic dye. Therefore, the photocatalytic process will be easier. As the pH increases, electrostatic attraction of surface becomes less and decolorization decreases. In alkaline condition, the production of OH^\bullet radical increases. On the other hand, the surface of photocatalyst becomes negatively charged in alkaline medium. Fig. 7 reveals that the competition between these two conditions ultimately leads to a decrease in decolorization [31].

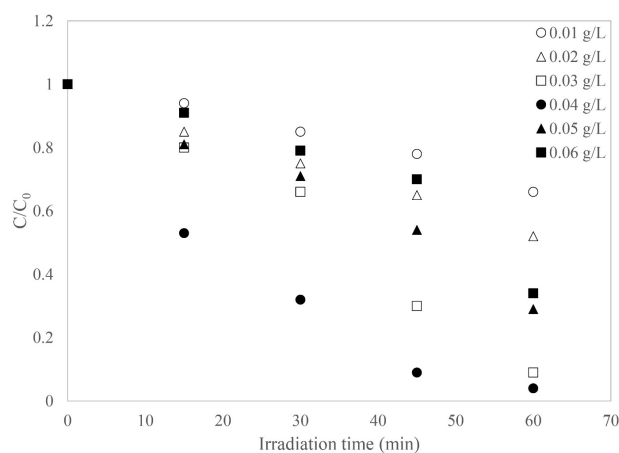


Fig. 6. Effect of photocatalyst concentration on the decolorization of indigo carmine at different irradiation times (stirring rate: 600 rpm; pH: 3; dye concentration: 5 ppm; Temperature: 27°C; UV lamp: 15 W).

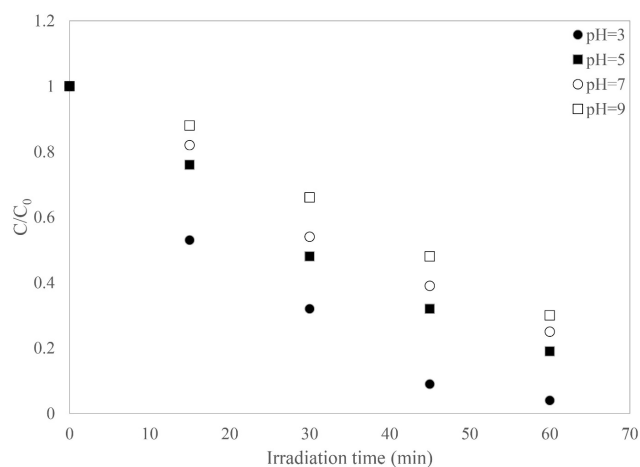


Fig. 7. Effect of pH on the decolorization of indigo carmine (photocatalyst concentration: 0.04 g/L; stirring rate: 600 rpm; dye concentration: 5 ppm; Temperature: 27°C; UV lamp: 15 W).

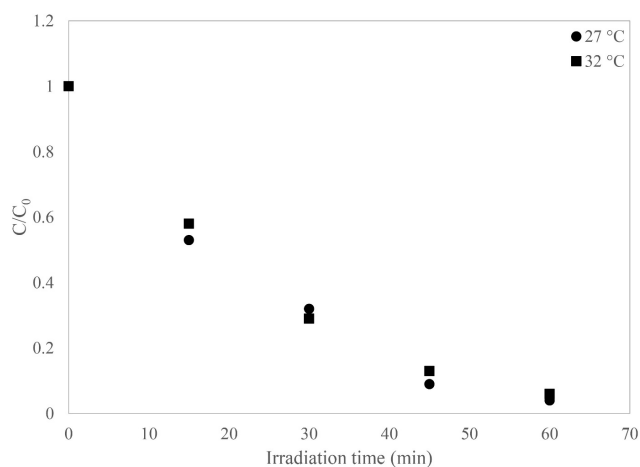


Fig. 8. Effect of temperature on the decolorization of indigo carmine (photocatalyst concentration: 0.04 g/L; stirring rate: 600 rpm; pH: 3; dye concentration: 5 ppm; UV lamp: 15 W).

4.3. Effect of temperature

The effect of temperature on the decolorization of dye at different irradiation time is illustrated in Fig. 8. According to the other researches, the temperature is supposed to have a positive effect on the dye degradation [32], but, it was observed that the rise in temperature in the range of 27–32°C had no significant effect on the dye removal. However, due to the energy consumption, 27°C was chosen as the optimal temperature for dye decolorization.

4.4. Effect of stirring rate

Fig. 9 shows variation of decolorization versus stirring rate. As can be seen, the dye decolorization increased as the stirring rate increased. Such an observation can be due to the fact that, the interaction of photons and silica-calcium zirconate photocatalyst increases at higher stirring rates. It should also be considered that higher stirring rate leads to higher aeration rate. As a result, the amount of oxygen available for decolorization also increases.

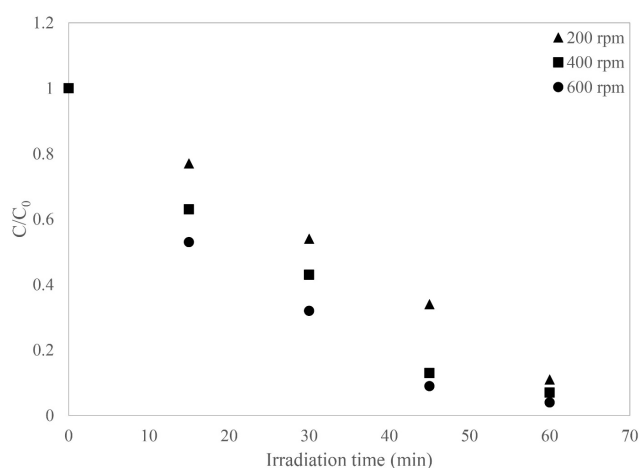


Fig. 9. Effect of stirring rate on the decolorization of indigo carmine (photocatalyst concentration: 0.04 g/L; pH: 3; dye concentration: 5 ppm; Temperature: 27°C; UV lamp: 15 W).

4.5. Effect of initial dye concentration on decolorization

Fig. 10 illustrates the plot of decolorization efficiency as a function of UV light irradiation time with various initial indigo carmine concentrations (5, 10, 20, and 30 ppm). It can be seen that the photocatalytic efficiency decreases as the dye concentration increases. As a result, with the increase of initial dye concentration, fewer protons can reach the surface of photocatalyst. Moreover, such an increase reduces the formation of OH^\bullet , $\text{O}_2^{\bullet-}$, and H_2O_2 radicals leading to lower radical/ dye ratio. Thus, the dye removal efficiency decreased. It must be noticed also that at higher concentrations of dye, the excess amount of pollutant at the photocatalyst surface reduces the access of active sites for photocatalytic degradation [33,34].

The pseudo-first order equation was used to describes the kinetics of decolorization:

$$\ln\left(\frac{C_0}{C}\right) = k_{app}t \quad (3)$$

where k_{app} is the apparent reaction rate constant (min^{-1}), t is the irradiation time (min) [35]. As it can be seen in Fig. 11, the correlation coefficient values are 0.9497 to 0.9801, which suggests a relatively strong relationship between parameters and also explains that the decolorization process of indigo carmine follows the pseudo-first order kinetics.

4.6. Energy consumption

Since the energy consumption plays a vital role in the reduction of operation cost, it is important to evaluate this energy. An estimation of photocatalyst energy consumption (kWh/m^3) was calculated using the following equation [36]:

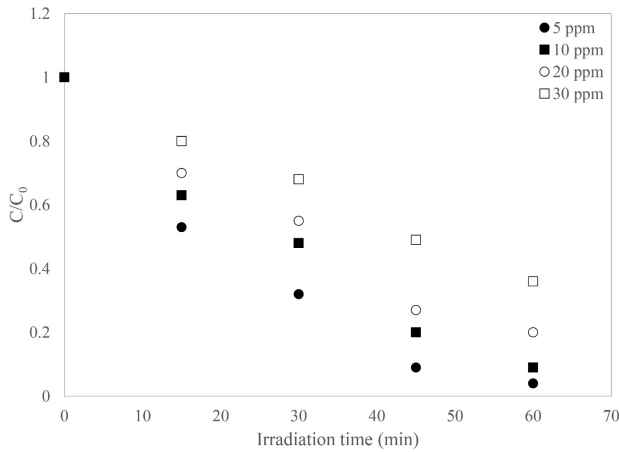


Fig. 10. Effect of initial dye concentration on the decolorization of indigo carmine (photocatalyst concentration: 0.04 g/L; stirring rate: 600 rpm; pH: 3; Temperature: 27°C; UV lamp: 15 W).

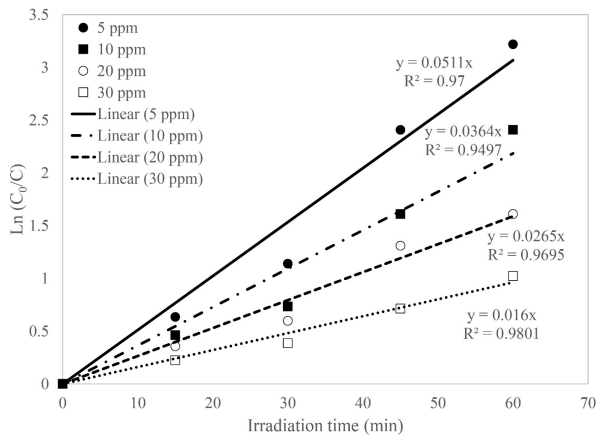


Fig. 11. Kinetic plot of the decolorization of indigo carmine at different initial dye concentration.

$$E_{EO} = \frac{38.4P_{el}}{V.K_{app}} \quad (4)$$

where P_{el} is the input power (kW) of the UV lamps, V is the volume of solution (L). As it can be seen in Table 2, the consumed energy for the maximum removal of Acid Blue74 after 60 min under the optimum conditions (dye concentration of 5 ppm, pH of 3 and photocatalyst concentration of 0.04 g/L), shows acceptable values for experimental and pilot applications (Table 2).

4.7. UV-Vis spectra of indigo carmine

Fig. 12 illustrates the UV-V is spectra of indigocarmin during the process of photocatalyticde colorization. As shown in Fig. 10, the adsorption peak at 610 nm corresponding to the azo group in Acid Blue 74 has disappeared, indicating the decolorization of indigo carmine. This figure shows various UV-V is spectra of Acid Blue 74 before and after 60 min of decolorization.

Table 2
Energy consumption of decolorization of acid blue 74

k_{app} (min ⁻¹)	C (mg/L)	E_{EO} (kwh/m ³)	Electricity price (\$/kwh)	Total cost (\$)
0.0511	5	5636.01	0.02	112.72
0.0364	10	7912.09	0.02	158.24
0.0265	20	10867.92	0.02	217.36
0.016	30	18000	0.02	360

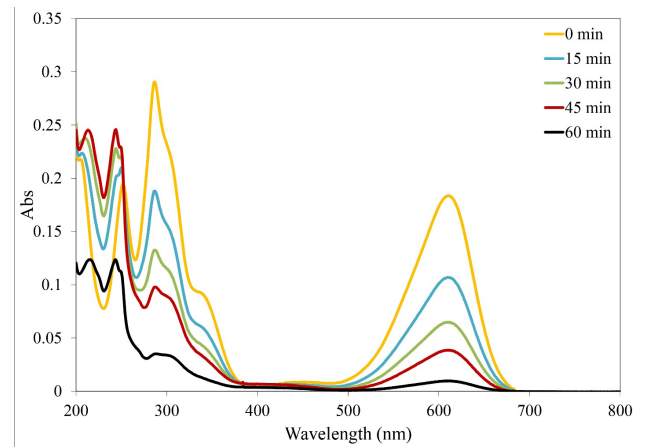
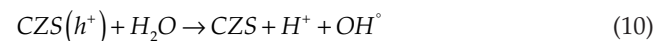
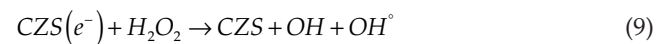
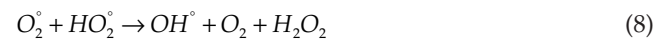
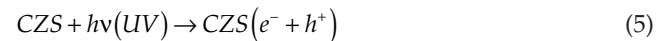


Fig. 12. Absorbance spectra of indigo carmine (photocatalyst concentration: 0.04 g/L; stirring rate: 600 rpm; pH: 3; dye concentration: 5 ppm; Temperature: 27°C; UV lamp: 15 W).

4.8. Mechanism of dye decolorization

The possible mechanism of the photocatalyticde colorization of AcidBlue 74 is as follows; First the photocatalyst is exposed to UV irradiation with an energy equal or greater than its band gap energy (3.3 eV) and thus the electrons on $CaZrO_3 - SiO_2(CZS)$ surface excited from valence band to conduction band resulting in electron/hole pairs formation and free electrons in the empty conduction band:



In the above-mentioned mechanism, e^- and h^+ are the electron-hole pairs in the conduction band and valence band, respectively. The e^- entity migrates to the surface of

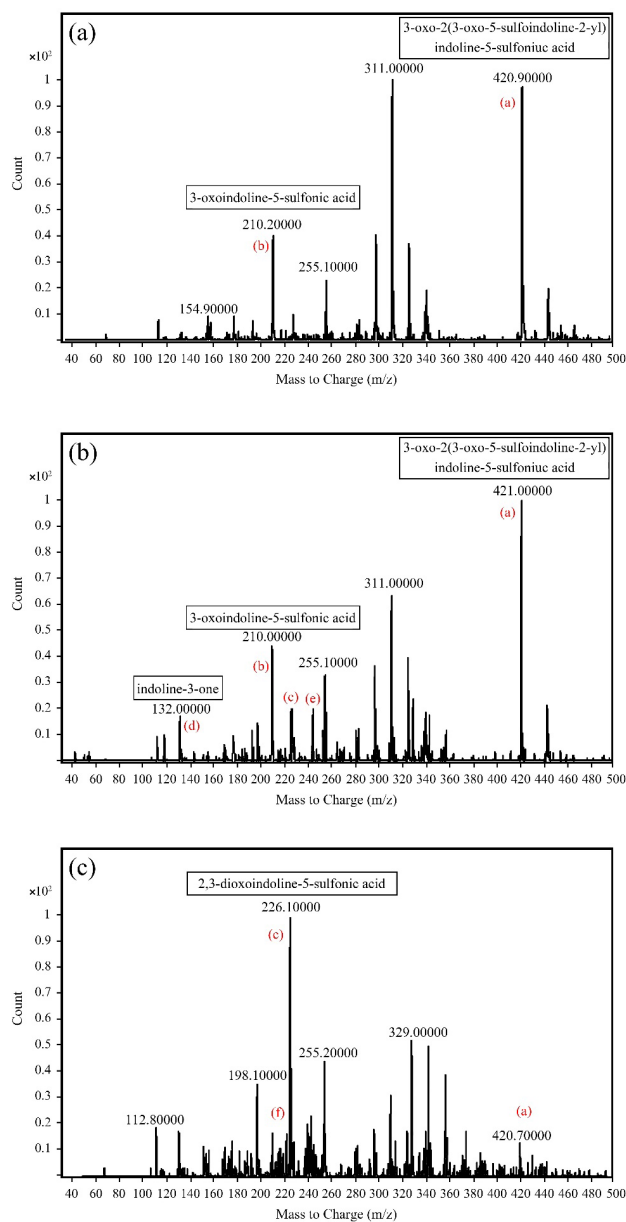


Fig. 13. The LC/MS profile of indigo carmine before photocatalytic (A), after 30 min of photocatalytic (B), and after 60 min of photocatalytic (C) process (photocatalyst concentration: 0.04 g/L; stirring rate: 600 rpm; pH: 3; dye concentration: 5 ppm; Temperature: 27°C; UV lamp: 15 W).

the photocatalyst where it can enter a redox reaction, react with the oxygen of the surface and generate OH radicals. The hole(h^+) in photocatalyst, which has a high oxidative potential, interacts with water and forms OH^\bullet radicals. The generated OH^\bullet radicals react with synthetic dye and produce H_2O , and CO_2 [37–39].

4.9. LC/MS analysis

In order to better understand the degradation of acid blue 74 using CZS/UV, LC/MS study was performed.

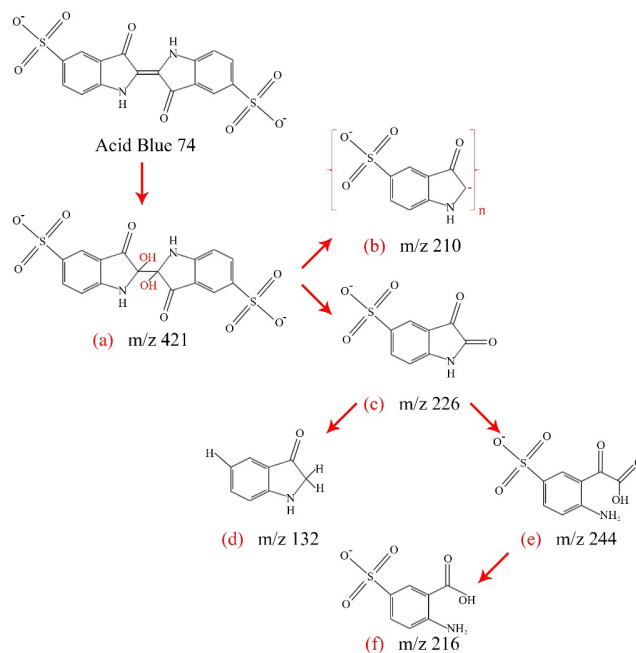


Fig. 14. Proposed pathway of indigo carmine decolorization with silica-calcium zirconate nanocomposite.

Fig. 13 shows the chromatographic behavior of the dye solution during several reaction time periods under the optimum experiment conditions maintained above. For the samples taken at longer reaction times, peaks were observed, indicating the decomposition of the dye and the concurrent formation of a group of intermediates. The explanation of this process is that the radical hydroxyl reacts with the carbon atom bearing the dye leakage, leading to cleavage of the C–C bond and the generation of is a tin 5-sulfonic acid (m/z 226), indolin-3-one (m/z 132), 3-oxoindoline-5-sulfonic acid [$M-Na$] $^{-2}$ (m/z 210). These are the products of decomposition of one of the contaminants present in the original sample: Indigo Carmine [$M-2Na+H$] (m/z 421). The chromatogram also reveals that the concentration of these compounds was insignificant after an hour of treatment [40,41]. The proposed pathway of decolorization illustrated in Fig. 14.

5. Conclusion

In this paper, silica-calcium zirconate nanocomposite was prepared and its photocatalytic efficiency for the degradation of indigo carmine in a batch reactor under UV light was investigated. The operating parameters were optimized and the effect of these parameters on the decolorization process was evaluated as well. It was observed that an optimum decolorization yield of 96% for acid blue 74 under the following conditions: photocatalyst concentration of 0.04 g/L, pH of 3, stirring rate of 600 rpm and initial dye concentration of 0.05 ppm. According to the above mentioned results, it can be concluded that silica-calcium zirconate nanocomposite is a suitable material for photocatalytic decolorization of dyes.

Acknowledgement

This work has been financially supported by the vice-chancellor for research of University of Torbat-e Jam.

Symbols

A	— Linear absorption coefficient of the substance
$h\nu$	— Photon energy
C_1	— Proportionality constant
E_g	— Band gap energy
C_0	— Concentration of dye before photocatalysis
C	— Concentration of dye after photocatalysis
E_{EO}	— Photocatalyst energy consumption
P^{el}	— Input power of the UV lamps
V	— Volume of solution
k_{app}	— Apparent reaction rate constant
e^-	— Electron in the conduction band
h^+	— Hole in the valence band

References

- [1] P. Kumar, R. Agnihotri, K.L. Wasewar, H. Uslu, C.K. Yoo, Status of adsorptive removal of dye from textile industry effluent, *Desal. Water Treat.*, 50 (2012) 226–244.
- [2] C.R. Holkar, A.J. Jadhav, D.V. Pinjari, N.M. Mahamuni, A.B. Pandit, A critical review on textile wastewater treatments: Possible approaches, *J. Environ. Manage.*, 182 (2016) 351–366.
- [3] K. Yamjala, M. SubramaniaNainar, N. Rao Ramiseti, Methods for the analysis of azo dyes employed in food industry – A review, *Food Chem.*, 192 (2016) 813–824.
- [4] M. Shabandokht, E. Binaeian, H. Tayebi, Adsorption of food dye Acid red 18 onto polyaniline-modified rice husk composite: isotherm and kinetic analysis, *Desal. Water Treat.*, 57(57) (2016) 27638–27650.
- [5] K.H. Kim, E. Kabir, S.A. Jahan, The use of personal hair dye and its implications for human health, *Environ. Int.*, 89–90 (2016) 222–227.
- [6] S. Dixit, A. Yadav, P.D. Dwivedi, M. Das, Toxic hazards of leather industry and technologies to combat threat: a review, *J. Clean. Prod.*, 87 (2015) 39–49.
- [7] M. Seggiani, M. Puccini, D. Castiello, N. Andreatini, P. Berni, S. Vitolo, Municipal wastewater reclamation and reuse in the leather industry, *Desal. Water Treat.*, 52(7–9) (2014) 1647–1653.
- [8] H.A. Shindy, Basics in colors, dyes and pigments chemistry: A review, *Chem. Int.*, 2(1) (2016) 29–36.
- [9] P. Huber, B. Carre, Decolorization of process water in deinking mills and similar applications: a review, *BioResources*, 7(1) (2012) 1366–1382.
- [10] U. Tezcan Un, S. Topal, F. Ates, Electrocoagulation of tissue paper wastewater and an evaluation of sludge for pyrolysis, *Desal. Water Treat.*, 57(59) (2016) 28724–28733.
- [11] J. Dasgupta, J. Sikder, S. Chakraborty, S. Curcio, E. Drioli, Remediation of textile effluents by membrane based treatment techniques: a state of the art review, *J. Environ. Manage.*, 147 (2015) 55–72.
- [12] J.M. Peralta-Hernandez, M.I. Maldondo, Y. MeasVong, F. Rodriguez, L.A. Godinez, S. Malato, Recent advances in the application of electro-fenton and photoelectron-fenton process for removal of synthetic dyes in wastewater treatment, *J. Environ. Eng. Manage.*, 19(5) (2009) 257–265.
- [13] M.D. Rutter, B.P. Saunders, G. Schofield, A. Forbes, A.B. Price, I.C. Talbot, Pancolonial indigo carmine dye spraying for the detection of dysplasia in ulcerative colitis, *Int. J. Hepatol. Gastroenterol.*, 53(2) (2004) 256–260.
- [14] C.F. Jabs, H.P. Drutz, The role of intraoperative cystoscopy in prolapse and incontinence surgery, *Am. J. Obstet. Gynecol.*, 185(6) (2001) 1368–1371.
- [15] A.K. Giri, T.S. Banerjee, G. Talukder, A. Sharma, Effects of dyes (indigo carmine, metanil yellow, fast green FCF) and nitrite in vivo on bone marrow chromosomes of mice, *Cancer Lett.*, 30(3) (1986) 315.
- [16] T. Robinson, G. McMullan, R. Marchant, P. Nigam, Remediation of dyes in textile effluent: a critical review on current, *Bioresour. Technol.*, 77(3) (2001) 247–255.
- [17] P. Asaithambi, R. Saravanathamizhan, M. Matheswaran, Kinetics studies of catalytic ozonation of distillery effluent, *Desal. Water Treat.*, 54(12) (2015) 3470–3476.
- [18] Z. Qin, S. Liu, S. Liang, Q. Kang, J. Wang, C. Zhao, Advanced treatment of pharmaceutical wastewater with combined micro-electrolysis, Fenton oxidation, and coagulation sedimentation method, *Desal. Water Treat.*, 57(53) (2016) 25369–25378.
- [19] A. Shrestha, M.A.H. Johir, S. Vigneswaran, J. Kandasamy, A comparative study on in-line flocculation and spiral flocculation followed by media filtration as a pre-treatment of seawater, *Desal. Water Treat.*, 55(22–24) (2015) 892–900.
- [20] B. AlHamad, N. Al-Bastaki, Degradation of Reactive Blue 19 using advanced oxidation methods: gliding-arc plasma discharge, *Desal. Water Treat.*, 57(51) (2016) 24352–24358.
- [21] C. Lopez, J. Martín-Pascual, J.C. Leyva-Díaz, M.V. Martínez-Toledo, M.M. Munio, J.M. Poyatos, Combined treatment of textile wastewater by coagulation–flocculation and advanced oxidation processes, *Desal. Water Treat.*, 57(30) (2016) 13987–13994.
- [22] F. Tisa, A. Abdul Raman, W.M.A Wan Daud, Applicability of fluidized bed reactor in recalcitrant compound degradation through advanced oxidation processes: a review, *J. Environ. Manage.*, 146 (2014) 260–275.
- [23] U.I. Gaya, A.H. Abdullah, Heterogeneous photocatalytic degradation of organic contaminants over titanium dioxide: A review of fundamentals, progress and problems, *J. Photochem. Photobiol. C*, 9(1) (2008) 1–12.
- [24] N. Yusoff, L.N. Ho, S.A. Ong, Y.S. Wong, W.F. Khalik, Photocatalytic activity of zinc oxide (ZnO) synthesized through different methods, *Desal. Water Treat.*, 57(27) (2016) 12496–12507.
- [25] A.K. Behera, C.V. Rao, R.K. Das, A.S. Giri, A.K. Golder, Fabrication and characterization of Ag-doped titania: impact of dye-sensitization, phenol decomposition kinetics and biodegradability index, *Desal. Water Treat.*, 57(20) (2016) 9488–9497.
- [26] N. Kermani, M. KargarRazi, S.S. Mirzaee, R. Tayebbe, Silica-calcium zirconate nanocomposite, studying its thermal and electrical properties, *B. Mater. Sci.*, 38(3) (2015) 673–678.
- [27] C.S. Prasanth, H.P. Kumar, R. Pazhani, S. Solomon, J.K. Thomas, Synthesis, characterization and microwave dielectric properties of nanocrystalline CaZrO₃ ceramics, *J. Alloy. Compd.*, 464 (2008) 306–309.
- [28] R. Al-Oweini, H. El-Rassy, Synthesis and characterization by FTIR spectroscopy of silica aerogels prepared using several Si(OR) and R⁺Si(OR⁻) precursors, *J. Mol. Struct.*, 919 (2009) 140–145.
- [29] S. Vangelista, R. Piagge, S. Ek, T. Sarnet, G. Ghidini, C. Martella, A. Lamperti, Structural, chemical and optical properties of cerium dioxide film prepared by atomic layer deposition on TiN and Si substrates, *Thin Solid Films*, 636 (2017) 78–84.
- [30] L. Favier, A.I. Simion, E. Matei, C.G. Grigoras, Y. Kadmi, A. Bouzaza, Photocatalytic oxidation of hazardous phenolic compound over TiO₂ in a batch system, *Environ. Eng. Manage. J.*, 15(5) (2016) 1059–1067.
- [31] S. Islam, S.K. Bormon, Md. Nadim, K. Hossain, A. Habib, T.S.A. Islam, Photocatalytic degradation of p-Nitrophenol (PNP) in aqueous suspension of TiO₂, *Am. J. Anal. Chem.*, 5 (2014) 483–489.
- [32] Q. Hu, B. Liuzhengzhong, Z. Mingxia, M. Song, X. Zhao, Temperature effect on the photocatalytic degradation of methyl orange under UV-vis light irradiation, *J. Wuhan Univ. Technol.*, 25(2) (2010) 210–213.
- [33] L. Favier, A.I. Simion, L. Rusu, M.L. Pacala, C. Grigoras, A. Bouzaza, Removal of an organic refractory compound by Photocatalysis in batch reactor- kinetic studies, *Environ. Eng. Manage. J.*, 14(6) (2015) 1327–1338.
- [34] L. Khenniche, L. Favier, A. Bouzaza, F. Fourcade, F. Aissani, A. Amrane, Photocatalytic degradation of bezacryl yellow in batch reactors – feasibility of the combination of photocatalysis and a biological treatment, *Environ. Tech.*, 36(1) (2015) 1–10.

- [35] A. Elhalil, R. Elmoubarki, M. Sadiq, M. Abdennouri, Y. Kadmi, L. Favier, S. Qourzal, N. Barka, Enhanced photocatalytic degradation of caffeine as a model pharmaceutical pollutant by Ag-ZnO-Al₂O₃ nanocomposite, *Desal. Water Treat.*, 94 (2017) 254–262.
- [36] J.R. Bolton, K.G. Bircher, W. Tumas, C.A. Tolman, Figures-of-merit for the technical development and application of advanced oxidation technologies for both electric- and solar-driven systems, *Pure Appl. Chem.*, 73(4) (2001) 627–637.
- [37] E.B. Gracien, J. Shen, X.R. Sun, D. Liu M. Li, S.D. Yao, J. Sun, Photocatalytic activity of manganese, chromium and cobalt-doped anatase titanium dioxide nanoporous electrodes produced by re-anodization method, *Thin Solid Films*, 515(13) (2007) 5287–5297.
- [38] H.R. Pouretedala, A. Norozi, M.H. Keshavarza, A. Semnani, Nanoparticles of zinc sulfide doped with manganese, nickel and copper as nanophotocatalyst in the degradation of organic dyes, *J. Hazard. Mater.*, 162 (2009) 674–681.
- [39] H.Y. Hea, C.Y. Tian, Rapid photo- and photo-Fenton-like catalytic removals of malachite green in aqueous solution on undoped and doped TiO₂ nanotubes, *Desal. Water Treat.*, 57 (31) (2015) 1–10.
- [40] C. Flox, S. Ammar, C. Arias, E. Brillas, A.V. Vargas-Zavala, R. Abdelhedi, Electro-Fenton and photoelectro-Fenton degradation of indigo carmine in acidic aqueous medium, *Appl. Catal. B: Environ.*, 67(1) (2006) 93–104.
- [41] M. Zaied, E. Chutet, S. Peulon, N. Bellakhal, B. Desmazieres, M. Dachraoui, A. Chausse, Spontaneous oxidative degradation of indigo carmine by thin films of birnessite electrodeposited onto SnO₂, *Appl. Catal. B: Environ.*, 107(1) (2011) 42–51.